

## Extended EOF Analysis of Tropical Disturbances: TOGA COARE

KLAUS FRAEDRICH

*Meteorologisches Institut, Universität Hamburg, Hamburg, Germany*

JOHN L. MCBRIDE

*Bureau of Meteorology Research Centre, Melbourne, Victoria, Australia*

WILLIAM M. FRANK

*Department of Meteorology, The Pennsylvania State University, University Park, Pennsylvania*

RISHENG WANG

*Meteorologisches Institut, Universität Hamburg, Hamburg, Germany*

(Manuscript received 11 March 1996, in final form 18 March 1997)

### ABSTRACT

Empirical orthogonal function (EOF) analyses are performed of time–height series of zonal and meridional winds and of cumulonimbus heating and drying in the Tropics. The data are from a rawinsonde array in the western Pacific located between the equator and 10°S during the intensive observation period of the Tropical Ocean Global Atmosphere Coupled Ocean–Atmosphere Response Experiment (TOGA COARE). The EOF analyses are performed by applying a window of 20 days to the data and thus calculating the EOFs of the time development of the vertical structure.

The wind time series is found to be well represented by two pairs of EOFs, each representing an oscillation. The first oscillation has a period of approximately 40 days, is predominantly in the zonal wind component, and has a first internal mode vertical structure with westerly anomalies in the lower troposphere corresponding to easterly perturbations in the upper troposphere. This pair describes 48.3% of the variance. A second EOF pair in the wind is a zonal variation that occurs predominantly in the upper troposphere. It has a period of approximately 24 days and describes 13.9% of the variance.

The heating–drying series is described by a dominant oscillation of period 40 days representing 41% of the variance. The structure is maximum in the middle troposphere and is associated with the same physical phenomenon as the dominant ( $u$ ,  $v$ ) oscillation. The second EOF pair for heating–drying has a period of 13 days, so there is a large time separation in periodicities for heating–drying compared to that for winds. The second (13 day) oscillation in heating–drying has the same vertical structure as the dominant (40 day) oscillation.

### 1. Introduction

The goals of the current study are 1) to demonstrate the utility of the windowed vertical time delay EOF analyses (Fraedrich et al. 1993) in determining the modes of vertical and temporal variation of the tropical atmosphere, and 2) to determine the dominant modes of wind and diabatic heating variation in the equatorial Western Pacific during TOGA COARE (Tropical Ocean Global Atmosphere Coupled Ocean–Atmosphere Response Experiment).

One of the themes of tropical meteorology research

in recent decades has been the determination of the relationship between variations in latent heat release and in the large-scale flow. To that end radiosonde data have been used from a number of tropical field experiments to measure the structure and variations in the diabatic and subgrid-scale heat source ( $Q_1$ ) and in the physically associated moisture sink ( $Q_2$ ). Examples include measurements in the GATE 1974 experiment in the tropical Atlantic by Thompson et al. (1979) and by Song and Frank (1983); in the winter MONEX 1978 experiment in the South China Sea by Johnson and Young (1983); in the AMEX 1987 experiment north of Australia by McBride et al. (1989) and Frank and McBride (1989); and in the TAMEX 1987 experiment near Taiwan by Johnson and Bresch (1991).

For various reasons related to data quality and quantity, the emphasis in the above studies has been on the

---

*Corresponding author address:* Klaus Fraedrich Meteorologisches Institut, Universität Hamburg, Bundesstraße 55, D-20146 Hamburg, Germany  
E-mail: fraedrich@dkrz.de

determination of the time-averaged flow and vertical distribution of the heating and drying. The recent TOGA COARE 1992–93 experiment in the tropical Western Pacific has provided a tropical radiosonde dataset of unprecedented quality extending over a 120-day period. This provides the opportunity to determine the vertical and temporal structure of both the wind fields and the heating and drying fields.

The method of analysis used in this note is the extended EOF (empirical orthogonal function) technique used by Fraedrich et al. (1993) and Wang et al. (1995) for the analysis of stratospheric wind data. Traditional EOF analyses of the vertical distribution of tropical heating and drying have been carried out previously by Alexander et al. (1993) and by Frank et al. (1996). The extended EOF method adds a time dimension to the vector being analyzed so that the temporal evolution is included when determining the principal modes of variation. As there are two or three cycles of the Madden–Julian oscillation (Madden and Julian 1971, 1972, 1994) observed during the intensive observing period (IOP), the analysis is focused on the coherent vertical time structure of the wind and heating fields of these cycles. This structure is represented by the first pair of time–height EOF modes. The technique is applied to a 120-day time series of wind and temperature measurements, as described in section 2. The results are presented in section 3, where we describe the vertical structure and periods of the two dominating EOF modes and their relationships to each other. That section also contains some physical interpretation of the EOF modes. Higher order modes are described in the appendix. Section 4 summarizes the main findings.

## 2. Data and methodology

### a. Acquisition and preparation of the dataset

The analyses are performed using observations from the TOGA COARE IOP, which lasted from 1 November 1992 to 28 February 1993. The primary data source is a set of rawinsonde soundings at seven stations in the equatorial west Pacific (Fig. 1). This rawinsonde array was referred to by Frank et al. (1996) as the OSA–S (Outer Sounding Array–South). The data were extracted from the Australian Bureau of Meteorology TAPS (Tropical Analysis and Prediction System) files. Additional data were obtained after the IOP and were added to the dataset. These included some data from six ISS (Integrated Sounding System) island and ship stations, obtained from the National Center for Atmospheric Research (NCAR), and many surface reports, which were primarily retrieved from archive tapes at the National Climate Center of the Bureau of Meteorology. A more complete description of these data and their initial analysis is presented in Frank et al. (1996).

All soundings were subjected to a series of quality control tests to remove highly suspicious data points.

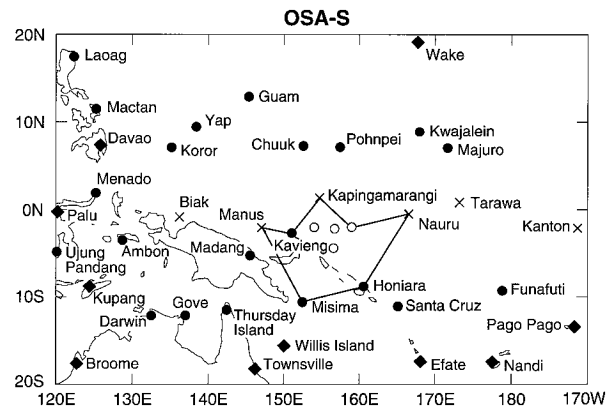


FIG. 1. The OSA–S rawinsonde array (solid line) of TOGA COARE stations (from Frank et al. 1996) over which the heating, drying, and wind time series are calculated.

Surface wind speeds were estimated as 72% of the winds at 850 hPa to remove unrealistic reductions of the surface winds at island stations, as discussed by Frank et al. (1996). Surface specific humidity ( $q$ ) values at two stations were adjusted after intercomparison with ship data, as outlined in Frank et al. (1996). Although the soundings were launched at 6-h intervals, there were many missing data points, and all data were averaged over 24 h to produce daily mean values. Only data from the 11 standard levels were used. These are surface, 1000, 850, 700, 500, 400, 300, 250, 200, 150, and 100 hPa. About 5% of the daily averaged values were missing, and these were filled in by applying a horizontal linear fit to a plane of least squares following the method of Frank (1979). The above procedure produced a complete dataset at all stations and at all 11 analysis levels for the 120 days of the IOP.

Heat and moisture budgets were computed for the area OSA–S outlined in Fig. 1 for each day, using the line integral procedure of McBride et al. (1989) with the modification in flux computations introduced by Molinari and Skubis (1988). Frank et al. (1996) compared the heat and moisture budgets for the array with independent measurements and concluded that the rawinsonde dataset is of good quality when analyses are averaged over periods of a day or longer.

In the current study the daily array-averaged values of four variables at the 11 levels are analyzed. The variables are the zonal and meridional wind components ( $u$  and  $v$ ) and the apparent heat source ( $Q_1$ ) and apparent moisture sink ( $Q_2$ ) defined by Yanai et al. (1973). Briefly, the latter two quantities represent, respectively, the net unresolved-scale heating of the array (due to condensation, radiation, and vertical eddy fluxes) and the net removal of moisture from the array (due primarily to convective rainfall) at each level.

Since the budgets are computed for 24-h periods over a relatively large area, they resolve the net effects of many clouds and mesoscale convective systems aver-

aged over their cumulative life cycles. Higher-order effects of individual convective systems are significantly smoothed by this averaging.

#### *b. The large-scale flow during TOGA COARE*

The evolution of the large-scale weather patterns during the TOGA COARE IOP has been described by several authors including Gutzler et al. (1994), McBride et al. (1995), and Chen et al. (1996). The area of analysis of the current study, which lies roughly within Area D of McBride et al., experienced increasing convective activity during the 4-month period of the IOP due to the normal seasonal evolution of the flow in this region. As described by McBride et al., the Southern Hemisphere monsoon became established in the region south of the equator by late November 1992. The monsoon circulation of the Southern Hemisphere extended farther eastward than normal during this year, which was associated with the warm phase of an ENSO event (Gutzler et al. 1994).

Both the convection and the low-level zonal winds were strongly affected by the occurrence of a 40–50-day Madden–Julian low-frequency wave. This wave resulted in two periods of active convection and strong westerly surface winds; the first was during late December 1992–early January 1993, and the second was during late January through most of February 1993. Between these periods there was an inactive or “break” period with low-level easterly flow and suppressed convection.

McBride et al. (1995) documented that the flow patterns at frequencies higher than the Madden–Julian wave were strongly influenced by the life cycles and movements of tropical cyclones in both the Northern and Southern Hemispheres. A number of authors have identified equatorial wave modes in the flow as predicted by the equatorial  $\beta$ -plane shallow water theory of Matsuno (1966). In particular, using 6–30-day bandpass-filtered wind, height, and outgoing longwave radiation (OLR) analyses, Kiladis and Wheeler (1995) documented disturbances during the IOP with characteristics of the equatorially trapped  $n = 1$  Rossby mode. These disturbances had an equivalent barotropic structure, but with maximum amplitude in the lower troposphere, and were associated with a periodicity in the flow on the order of 12 days. Numaguti (1995) found a similar mode, though he associated it with a baroclinic structure and a signal of approximately 15–20 days in period. Numaguti also presented evidence for equatorial disturbances of 4–5 days’ period, with the structure of a lower tropospheric mixed Rossby–gravity wave. Nishi and Sumi (1995) found disturbances with structure very similar to an equatorial Kelvin wave. These systems occurred in the upper troposphere and lower stratosphere and had a period of approximately 20 days during the COARE IOP. Finally, Chen et al. (1996) studied the internal structure of the Madden–Julian episodes in

COARE. Among other findings, they showed that within the convectively active phase of the oscillation cloud clusters were frequently concentrated into westward-propagating disturbances with a local periodicity of approximately 2 days. They identified these disturbances with westward-propagating inertia gravity waves, as had been identified in pre-COARE studies by Takayabu (1994).

#### *c. Analysis procedure: Height–time delay structure or extended EOF analysis*

Traditional empirical orthogonal function (EOF) analysis utilizes a time series and examines the temporal behavior of spatial patterns. The EOF patterns describe the spatial structure; the amplitudes (or principal components) characterize its time evolution. The original dataset can be reconstructed by adding the evolution of individual EOF patterns of successively higher order to the mean.

The extended EOF analysis recognizes that the temporal evolution of the spatial patterns is an integral part of a system’s development. Consider a height–time section, which is commonly described by a vector of  $K$  components ordered according to height and evolving with time. Sliding a time window of length  $W$  over this vector time series leads to a new vector, whose components span a height–time section,  $K \times W$ , evolving in time (see Fig. 4 of Fraedrich et al. 1993). This vector represents the states of the system in a  $K \times W$  dimensional phase space spanned by time-delay coordinates. In this sense the vector representation of a spatially extended dynamical system evolving in time associates the time development with the spatial structure. The following points should be noted when applying this technique.

- Introducing a sliding window to a dataset leads to some smoothing depending on the window length  $w$ . A larger window provides a smoother reconstruction of the time series, especially when compared with  $w = 1$  (the traditional EOF analysis). An optimal choice of the window length  $w$  is suggested by the half-period of the largest signal. This resolves the signal with sufficient detail and, simultaneously, provides the required smoothing of the dataset. Space–time eigenmodes of smaller scale are resolved in the higher-order EOFs.
- Wavelike oscillations are represented by a pair of EOFs with similar eigenvalues, and the associated EOF patterns are shifted by a quarter wavelength (not unlike sine and cosine waves). The dial (phase portrait) of the amplitude pair shows a more or less regular circulation about the center.
- The advantage of space–time extended EOFs is the ability (a) to obtain dominant internally coherent patterns in both space and time and among different variables and (b) to distinguish oscillatory components

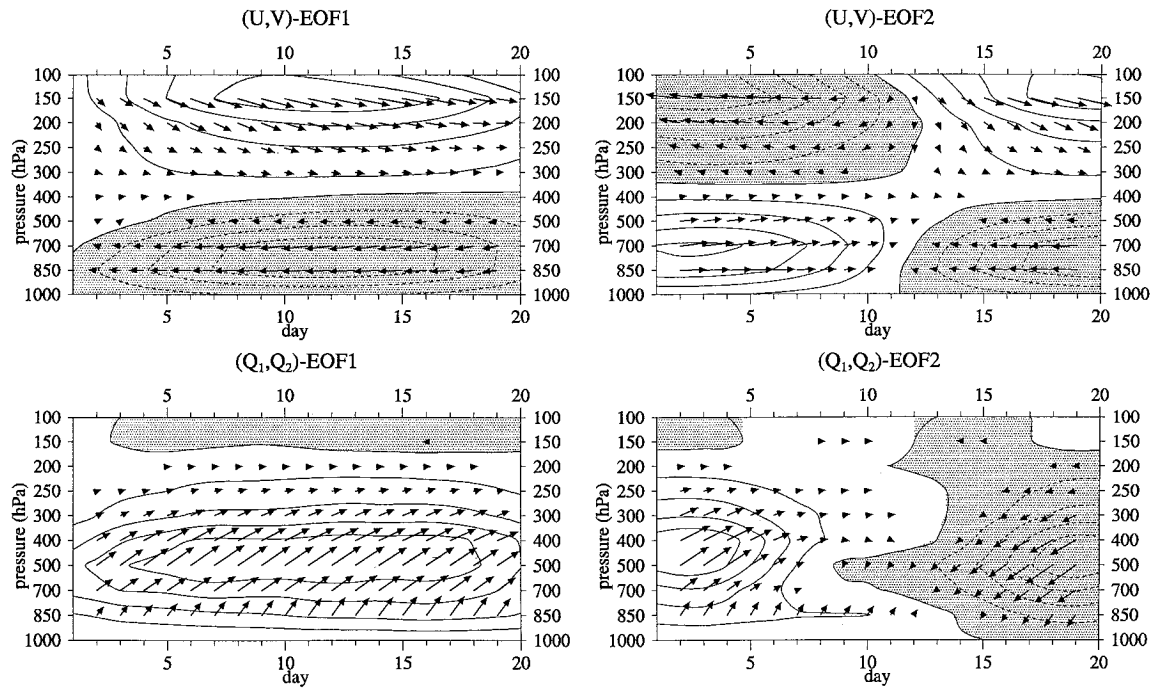


FIG. 2. The first EOF pairs of the  $(u, v)$  and the  $(Q_1, Q_2)$  height–time series with a 20-day window. Top panels: The vectors represent wind direction and strength. The contours are  $u$ -component (shaded negative); units are in meters per second. Bottom panels: The vectors represent  $(Q_1, Q_2)$  components with positive  $Q_1$  upward and positive  $Q_2$  to the right. The contours are  $Q_1$  component (shaded negative); the units are in degrees per day.

with various frequencies. They are characterized by pairs of EOFs in quadrature, which are associated with eigenvalues of similar magnitude; their time evolution is represented by a trajectory in a compact phase space spanned by these EOFs. This allows a closer and more precise analysis of the variability and of the mutual relation between the components.

As the 40–50-day Madden–Julian oscillation represents the largest scale of variability in the current dataset, this suggests the choice of a window of about 20–30 days. Indeed, tests with increasing window lengths (between 15 and 40 days) have shown that there are no significant changes in either the EOF patterns or the associated amplitudes; that is, the basic periods and the height–time structure remain unchanged and independent of window length. Therefore, the following dis-

cussion of the results of the extended EOF analysis will concentrate on a window of  $w = 20$  days.

### 3. Results

The first two EOFs of the covariance matrix of the  $(u, v)$  height–time series are shown in Fig. 2 (top). These two EOFs explain 48.3% of the variance (Table 1). Although the EOFs were computed using both  $u$  and  $v$ , the variations in  $u$  are much larger than those in  $v$  for each mode, and in Fig. 2 the  $u$  component of the wind is contoured. Wind vectors are plotted to show the total wind components of each mode.

EOF 1 shows a vertical wavenumber-one structure, with the zonal wind varying most near the tropopause and near 800 hPa. The structure of EOF 2 is virtually identical to that of EOF 1, but the phases are such that the two are in quadrature. This suggests the first two EOFs are a pair that represent a single mode of variation. This proves to be the case, as discussed below. The period of the oscillation corresponding to this pair can be estimated from the temporal structure as twice the time between successive maxima and minima. By inspection of Fig. 2 this is approximately twice the window length, or 40 days. This estimate will be refined later when we discuss the phase portraits (Fig. 3)

The first two modes of the  $(Q_1, Q_2)$  height–time series are shown in Fig. 2 (bottom), and their contributions to

TABLE 1. Percent variance (left) and the running total (right) contributed by the first six EOFs in the height–time delay analysis of the total  $(r, v)$  and  $(Q_1, Q_2)$  variance.

EOF	$(u, v)$	Wind	$(Q_1, Q_2)$	Heating
1	27.3	27.3	28.4	28.4
2	21.0	48.3	12.2	40.6
3	7.7	56.0	7.9	48.5
4	7.1	63.1	7.6	56.1
5	6.8	69.9	4.7	60.8
6	3.4	73.3	3.2	64.0

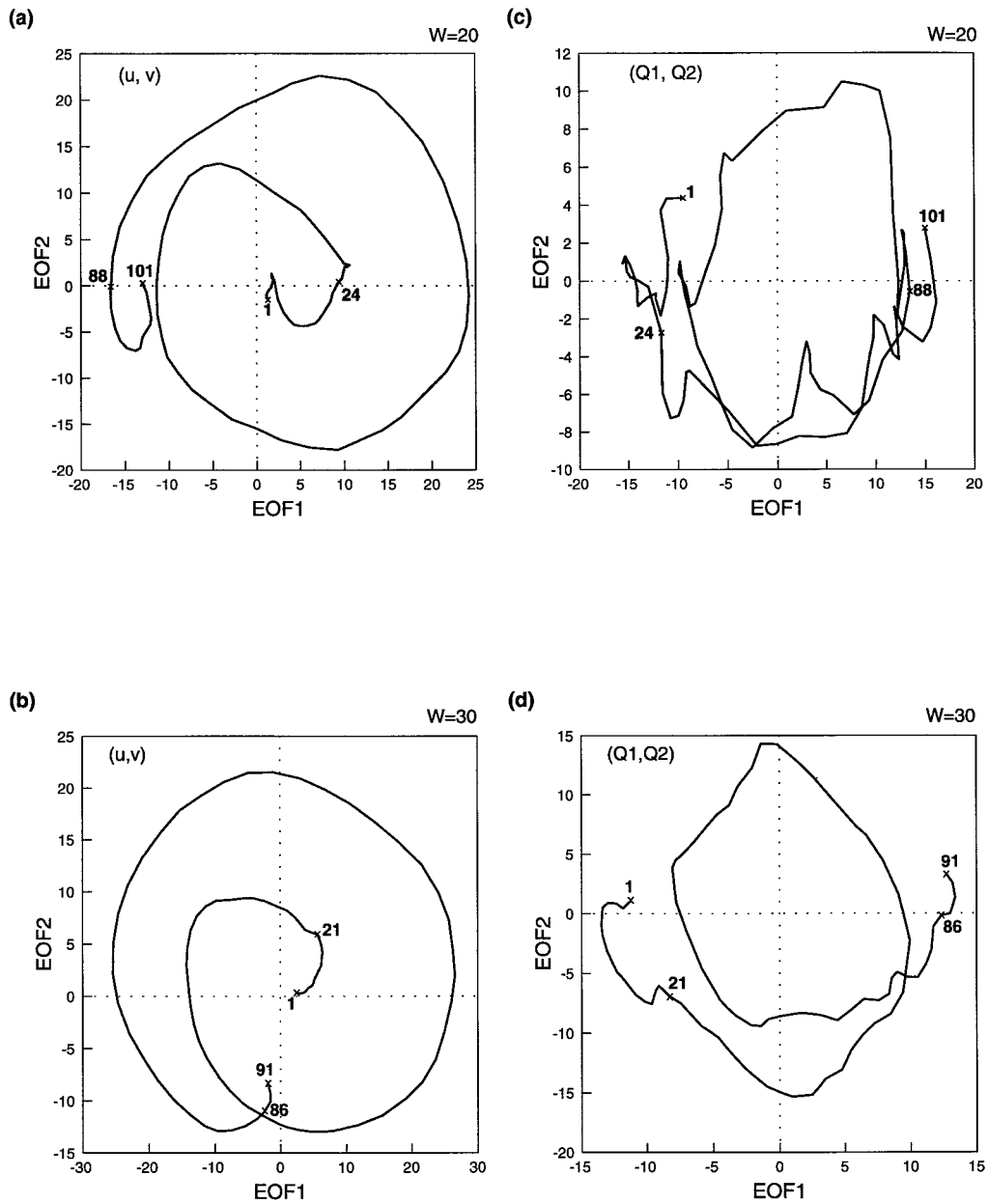


FIG. 3. Dial of the principal components of the first height–time delay eigenvector pair (EOF 1 and EOF 2) for the two window lengths ( $W = 20, 30$  days): (a), (b) the  $u, v$  winds and (c), (d) the  $(Q_1, Q_2)$  heating. Particular day numbers indicated are discussed in the text.

the variance are shown in Table 1. In this figure,  $Q_1$  is contoured. EOFs 1 and 2, which together explain 41% of the variance, are very similar to each other but are phase shifted. They show a simple vertical structure with maximum variability in the middle levels and minimum variability at the upper and lower boundaries. As with the first pair for  $(u, v)$ , the period can be estimated from the temporal structure as approximately twice the window length, that is, 40 days.

Since variations in  $Q_1$ , and to a somewhat lesser ex-

tent  $Q_2$ , are dominated by variations in the vertical velocity field, the vertical structure of these quantities corresponds to an internal wavenumber-one structure in divergence (not shown). It is remarkable that the same vertical structure persists for higher-order EOFs (see appendix). Thus the results show no significant variations in vertical heating structure corresponding to higher-order vertical wave modes resolvable from this dataset. As a check on the robustness of this result, the extended EOF analysis has been carried out on the di-

vergence fields with the same 20-day window. All conclusions concerning periodicities and vertical structure obtained by the extended EOF analysis of the derived fields ( $Q_1$ ,  $Q_2$ ) were substantiated by the analysis of the primary field (divergence).

The pairing of EOFs (1, 2) in wind and of (1, 2) in heating and drying is revealed in the phase portrait diagrams presented in Fig. 3. In each case the amplitude of one EOF is plotted against the amplitude of its pair. Since the members of each pair are similar in structure, each rotation in phase space represents a complete cycle through that pattern at the single station represented by the array average in Fig. 1.

The period of the oscillations is the time required for a complete revolution on these diagrams. For the first ( $u$ ,  $v$ ) pair (Fig. 3a), the upper axis is crossed at days 40 and 80, while the left axis is crossed at days (49, 88), giving a period of 39–40 days. By the same methods the first pair of ( $Q_1$ ,  $Q_2$ ) has a period of 41 days.

As stated in section 2, the results here are not oversensitive to the choice of window length. To demonstrate this, the same phase portraits are shown in Fig. 3 (bottom panel) for a window length of 30 days. For the ( $u$ ,  $v$ ) first pair the left axis is crossed at days 38 and 77, yielding a period of 39 days. For the ( $Q_1$ ,  $Q_2$ ) first pair, the lower axis crossings are at days 26 and 69, yielding a period 43 days. This consistency between the results for windows of 20 and 30 days shows that the periodicities and coherence found are robust and are not a harmonic of the window length chosen.

The extended EOF analysis has revealed a dominant pattern of variation in both wind and heating–drying sources with a period of approximately 40 days. This result is no surprise and has been discussed in the context of the COARE data by Gutzler et al. (1994) and McBride et al. (1995). Both sets of authors associated this variation with the Madden–Julian oscillation. The current analysis is consistent with the above results. The structure of this oscillation is seen in eigenvectors 1 and 2 of Fig. 2 to be dominated by zonal wind variations and to have the vertical structure of a tropospheric first internal mode. This zonal wind pattern is consistent with the structure of an equatorially trapped Kelvin wave but, as noted below, the mode is probably not totally a Kelvin wave.

Despite the fact that the ( $Q_1$ ,  $Q_2$ ) vector has been analyzed separately from the ( $u$ ,  $v$ ) vector, the variations described by the first EOF pair in each instance clearly represent the same phenomenon. Evidence for this can be found through further inspection of the phase portraits for this oscillation in Figs. 3a and 3b. The numbers on the trajectories are day numbers. It is seen that both first pairs remain relatively stationary in phase space for the first 24 days. They then undergo one-and-a-half revolutions until day 88. They then are quasi-stationary until the end of the series (day 101). The same behavior can be seen also on the 30-day window series (Figs. 3c,d); though with the longer window the series of over-

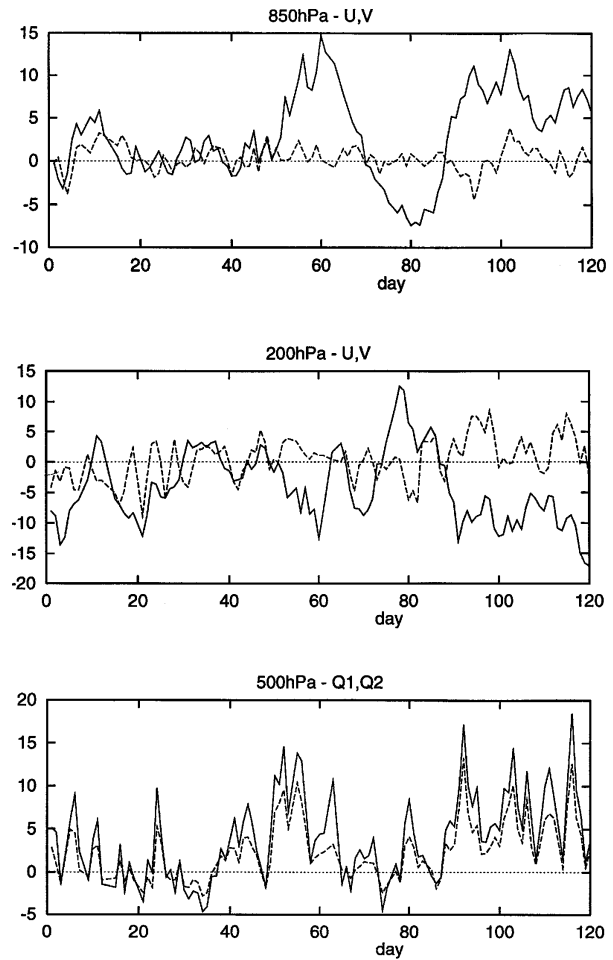


FIG. 4. Original time series of the zonal and meridional wind in 850- and 200-hPa levels ( $u$ ,  $v$ , full and dashed line in  $\text{m s}^{-1}$ ) and the  $Q_1$  heating at 500 hPa (full line, in  $\text{deg day}^{-1}$ ) and 500-hPa  $Q_2$  drying (dashed line,  $\text{deg day}^{-1}$ ).

lapping vectors in time has been shortened by 10 days, which has the effect of decreasing the lengths of the stationary periods that happen to occur at the beginning and end of the series.

Figure 4 shows the original time series of wind components ( $u$ ,  $v$ ) at 850 and 200 hPa, and heating and drying ( $Q_1$ ,  $Q_2$ ) at 500 hPa after removing linear trends computed from least squares regression. The trends for  $u(850)$ ,  $v(850)$ ,  $u(200)$ ,  $v(200)$ ,  $Q_1(500)$ , and  $Q_2(500)$  are  $+0.51 \text{ m s}^{-1} \text{ day}^{-1}$ ;  $-0.005 \text{ m s}^{-1} \text{ day}^{-1}$ ;  $-0.034 \text{ m s}^{-1} \text{ day}^{-1}$ ;  $+0.05 \text{ m s}^{-1} \text{ day}^{-1}$ ;  $+0.06^\circ\text{C day}^{-1}$ ;  $+0.04^\circ\text{C day}^{-1}$ , respectively. Figure 5 shows the same series as reconstructed from the first pair of EOFs. Comparison of the upper panels reveals the clear out-of-phase relationship between upper and lower levels. It also reveals that the oscillation is not totally a Kelvin wave structure, as there does exist an oscillation in the meridional wind at upper levels.

Since we have concluded the wind and heating–dry-

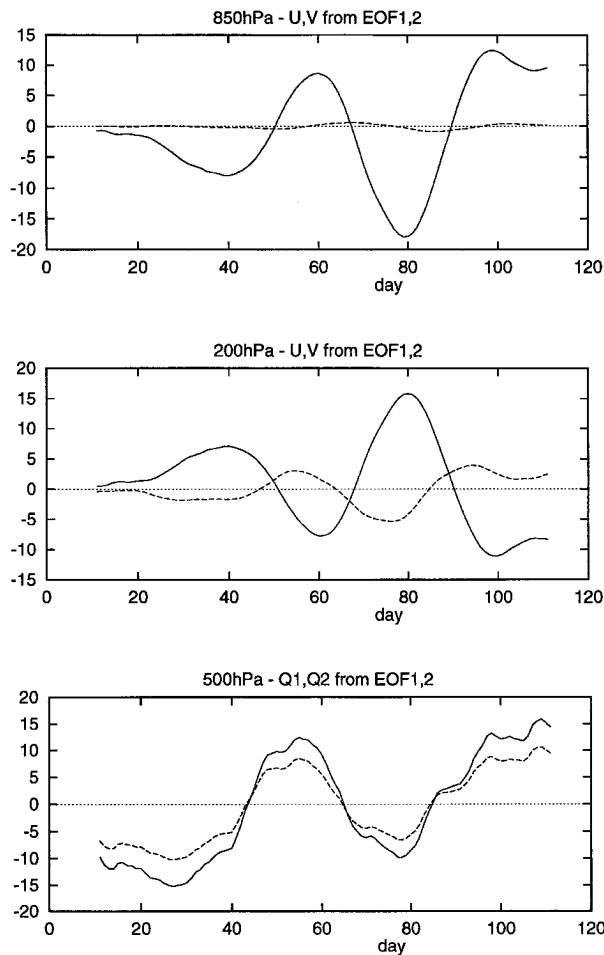


FIG. 5. Time series reconstructed from the first EOF pair of the zonal and meridional wind in 850- and 200-hPa levels ( $u$ ,  $v$ : full and dashed line in  $\text{m s}^{-1}$ ) and the  $Q_1$  heating at 500 hPa (full line, in  $\text{deg day}^{-1}$ ) and 500-hPa  $Q_2$  drying (dashed line,  $\text{deg day}^{-1}$ ).

ing oscillations represent the same phenomenon, it is appropriate to examine the phase relationships between the two sets of variables. From comparison of the lower panel of Fig. 5 with the upper two panels, it is seen that both the heating and zonal wind variations associated with this pair are dominated by one cycle beginning at about day 40 and continuing to the end of the experiment. The heating and drying maximum occur simultaneously and correspond to a maximum easterly perturbation in the upper troposphere and a maximum westerly perturbation in the lower troposphere. The zonal winds increase with or shortly after the onset of the heating, a result found previously by McBride et al. (1995).

The extended EOF analysis also reveals quadrature pairs for higher-order modes. Given the wide use of the TOGA COARE data the structure of these higher order periodicities is also worth recording. However, a referee of this paper disputes the significance of these pairs due

to a lack of separation of the eigenvalues, following the significance tests set out in the rule of thumb of North et al. (1982). We disagree with the referee, as the rule of thumb is relevant in the context of treating EOFs as a probability distribution property estimated from a set of samples derived from a parent distribution. Thus the basic concern of the rule of thumb is how well the estimated EOFs represent the “true EOFs.” In the current context the EOFs are being used in the context of dynamical system analysis. The basic concern is the characterization of space–time coherence involving patterns underlying certain wave motions. The problem of degeneracy does not enter, so the appropriate statistical tests would involve an analysis of the effect of observational errors on the EOF structures and periodicities. Such statistical testing procedures are beyond the scope of the current paper. Thus, due to the disagreement on the significance of these higher modes, a minimal description of them has been relegated to the appendix.

#### 4. Discussion

The extended EOF method has been applied to the heating rate and wind time–height series averaged over the OSA–S radiosonde array during the IOP of TOGA COARE. As with all EOF analyses it provides a concise description of the variations contained in the original time series. The advantage of the extended or “time-windowed” method is that it includes the time variation of the heating and wind as part of the vector being represented by the orthogonal functions. This has yielded a number of interesting results.

For the wind series, it is found that 48% of the variance can be described by a single EOF pair (representing an oscillation). This has a structure very similar to a tropospheric first internal mode Kelvin wave. The extended EOF methodology reveals a period for the oscillation equal to approximately 40 days. For the series of heating and drying, an oscillation of approximately 41 days accounts for 40.6% of the variance. The vertical structure shows the heating and drying variations maximum in the middle troposphere, as was found by conventional EOF analysis by Frank et al. (1996). From inspection of trajectories in phase space we conclude this oscillation represents the same phenomenon as the first pair in the wind-vector series. The zonal winds increase either coincident with or lagging by a few days increases in convective heating.

As a final comment, the extended EOF methodology has proved to be a useful technique for determining periodicities in the COARE wind and heating–drying time series. In particular, it presents a naturally designed filter to examine the dynamical structure of signals of various frequencies, so this procedure may present a useful alternative to compositing.

*Acknowledgments.* Comments by George Kiladis and two referees are appreciated. The following fellowships

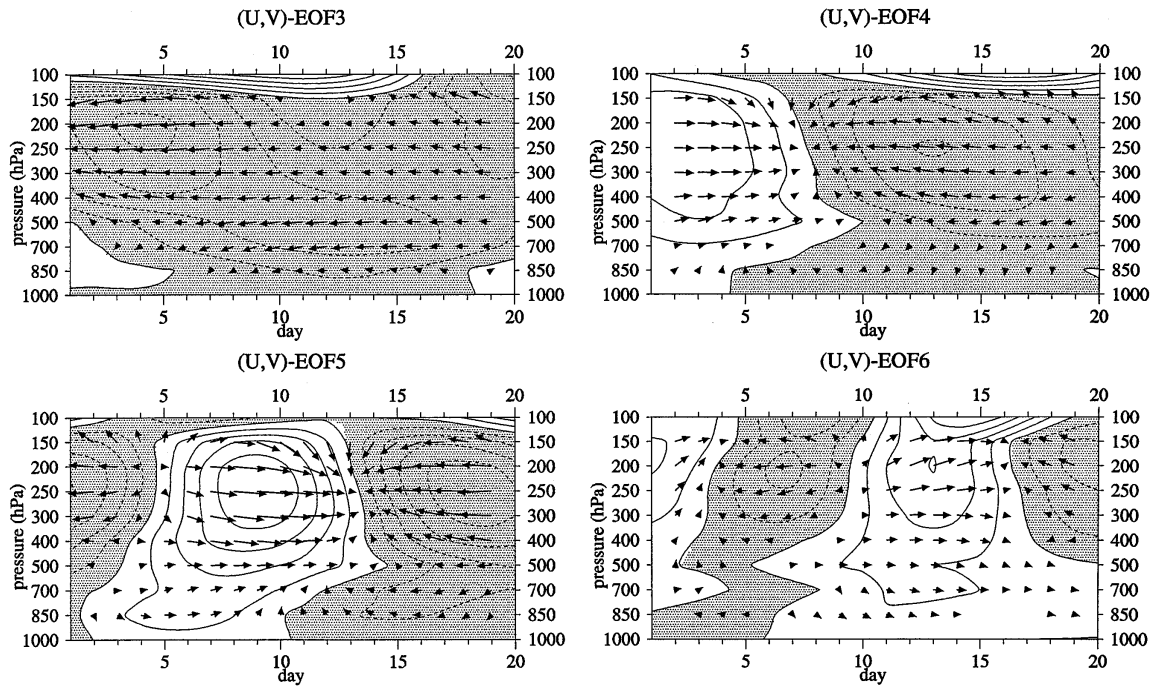


FIG. A1. The EOF 3–EOF 6 of the  $(u, v)$  height–time series with a 20-day window. The vectors represent wind direction and strength. The contours are  $u$  component (shaded negative); units are in meters per second.

contributed to this cooperation: Max-Planck Prize (K.F.), Fulbright (W.F.), and Humboldt (J.McB.). William Frank's COARE research was under NSF Grant ATM-911 59050, ONR Grant N00014-92J-1069, and the American–Australian Education Foundation. R. Wang was supported by a BMFT (Germany) Climate Research Grant.

#### APPENDIX

##### Higher-Order EOFs

The EOFs of higher order than the first pairs are of further interest and are discussed here. Figure A1 shows that the third  $(u, v)$  EOF, which explains about 8% of the variance, does not appear to form a pair with any other EOF. However, EOFs 4 and 5 are quite similar in structure and period. They both show variations in the zonal wind that extends through the depth of the troposphere with maximum variations in the upper levels, and they have periods of 20–25 days. They explain about 15% of the total variance between them. EOF 6 is a higher-frequency mode, with a period of about 10–12 days and maximum wind variations near the tropopause. It is a relatively weak mode, explaining only 3% of the variance. Figure A2 shows that the  $(Q_1, Q_2)$  EOFs 3 and 4 closely resemble each other but are phase shifted. They have the same vertical structure as all of the other EOF modes, as noted above, and they show a period of about 10–12 days. Together they explain about 16% of the variance. The pairing of EOFs (4, 5)

in wind and of (3, 4) in heating and drying is also revealed in the phase portrait diagrams (not shown). It is worth noting that similar pairings are found in higher-order eigenvectors. For both  $(u, v)$  and  $(Q_1, Q_2)$ , the next clear pairs are for EOFs 6 and 7. For  $(u, v)$  this set has an upper tropospheric structure, has a periodicity of the order of 7–8 days, and accounts for just over 6% of the variance. For  $(Q_1, Q_2)$  pair EOF 6, EOF 7 has a mid-tropospheric maximum, has a periodicity of 7–8 days, and also accounts for slightly over 6% of the variance. Furthermore, as stated in section 2, the results are not oversensitive to the choice of window length.

In summary, (a) a second pair of EOFs with a period of approximately 24 days explains a further 13.9% of the variance. This second oscillation also is found predominantly in the zonal wind. Its vertical structure shows the same sign throughout the depth of the troposphere but is much stronger at upper levels. Zonal wind oscillations of this period in the upper troposphere have been noted previously by Wallace (1971) and in the TOGA COARE data by Nishi and Sumi (1995). These latter authors identified these oscillations as being associated with an upper tropospheric–lower stratospheric equatorially trapped Kelvin wave. (b) In the case of the heating series, there is quite a large spectral gap to the second prominent oscillation. This is represented by a second pair (EOFs 3 and 4) representing 15.5% of the variance and with a period of approximately 13 days. Oscillations of this periodicity have been noted in (pre-TOGA COARE) tropical satellite cloud images by Tak-

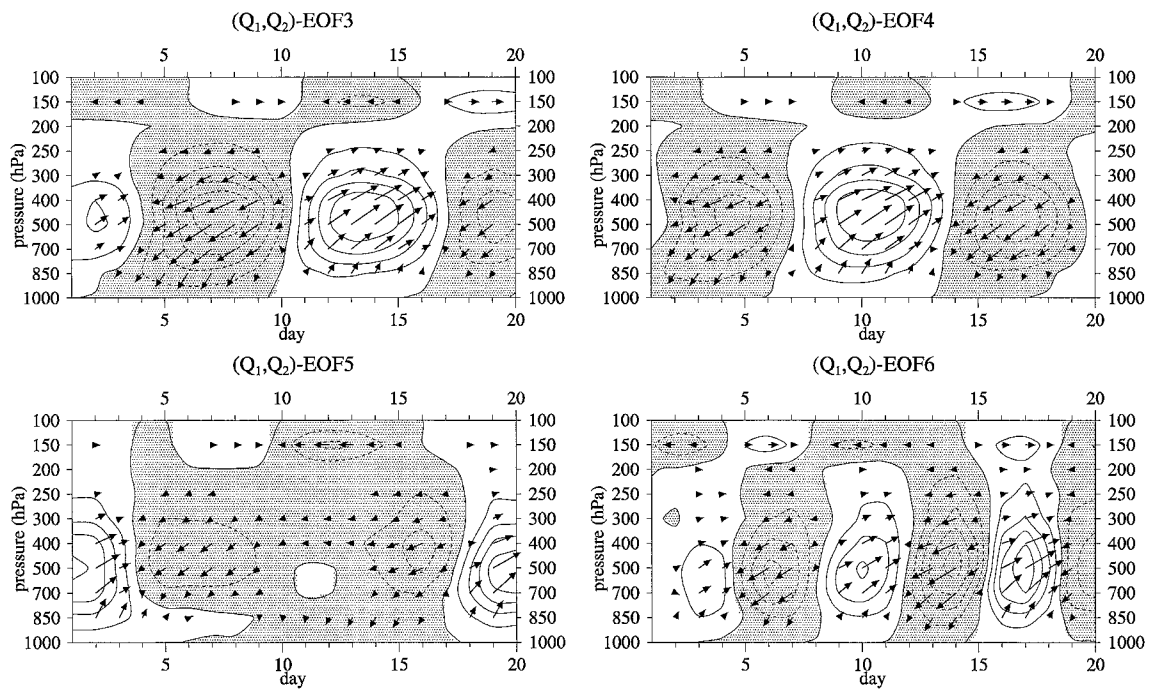


FIG. A2. The EOF 3–EOF 6 of the  $(Q_1, Q_2)$  height–time series with a 20-day window. The vectors represent  $(Q_1, Q_2)$  components with positive  $Q_1$  upward and positive  $Q_2$  to the right. The contours are  $Q_1$  component (shaded negative); the units are in degrees per day.

ayabu (1994), who associated them with equatorially trapped Rossby waves. Due to the “single-station” nature of the current analysis, however, we can offer neither support nor refutation of this interpretation. The vertical structure of the second EOF pair for the heating–drying is the same as that for the lower-frequency pair, that is, with a single maximum in the midtroposphere and tapering to zero both at the ground and near the tropopause. This heating structure corresponds to a simple lower tropospheric inflow, upper tropospheric outflow divergence profile; indeed, an independent extended EOF analysis simply of the divergence time series reveals the same periodicities and the same consistency in vertical structure between the higher- and lower-frequency oscillations (not shown). Following the results of Alexander et al. (1993), it is expected that the variance in cumulonimbus related sources  $Q_1, Q_2$  will attain a different vertical structure when oscillations close to 1 day are examined (e.g., the diurnal cycle).

#### REFERENCES

- Alexander, G. D., G. S. Young, and D. V. Ledvina, 1993: Principal component analysis of vertical profiles of  $Q_1$  and  $Q_2$  in the Tropics. *Mon. Wea. Rev.*, **121**, 535–548.
- Chen, S. S., R. A. Houze Jr., and B. E. Mapes, 1996: Multiscale variability of deep convection in relation to large-scale circulation in TOGA COARE. *J. Atmos. Sci.*, **53**, 1380–1409.
- Fraedrich, K., R. Wang, and S. Pawson, 1993: An EOF analysis of the vertical-time delay structure of the quasi-biennial oscillation. *J. Atmos. Sci.*, **50**, 3357–3365.
- Frank, W. M., 1979: Individual time period analyses over the GATE ship array. *Mon. Wea. Rev.*, **107**, 1600–1616.
- , and J. L. McBride, 1989: The vertical distribution of heating in AMEX and GATE cloud clusters. *J. Atmos. Sci.*, **46**, 3464–3478.
- , H. Wang, and J. L. McBride, 1996: Rawinsonde budget analyses during the TOGA COARE IOP. *J. Atmos. Sci.*, **53**, 1761–1780.
- Gutzler, D. S., G. N. Kiladis, G. A. Meehl, K. M. Weickmann, and M. Wheeler, 1994: Seasonal climate summary: The global climate of December 1992–February 1993. Part II: Large-scale variability across the tropical western Pacific during TOGA COARE. *J. Climate*, **7**, 1602–1622.
- Johnson, R. H., and G. S. Young, 1983: Heat and moisture budgets of tropical mesoscale anvil clouds. *J. Atmos. Sci.*, **40**, 2138–2147.
- , and J. F. Bresch, 1991: Diagnosed characteristics of precipitation systems over Taiwan during the May–June 1987 TAMEX. *Mon. Wea. Rev.*, **119**, 2540–2557.
- Kiladis, G. N., and M. Wheeler, 1995: Horizontal and vertical structure of observed tropospheric equatorial Rossby waves. *J. Geophys. Res.*, **100**(D11), 22 981–22 997.
- Madden, R. A., and P. R. Julian, 1971: Detection of a 40–50 day oscillation in the zonal wind in the tropical Pacific. *J. Atmos. Sci.*, **28**, 702–708.
- , and —, 1972: Description of global-scale circulation cells in the tropics with a 40–50 day period. *J. Atmos. Sci.*, **29**, 1109–1123.
- , and —, 1994: Observations of the 40–50-day oscillation—A review. *Mon. Wea. Rev.*, **122**, 814–837.
- Matsumo, T., 1966: Quasi-geostrophic motions in the equatorial area. *J. Meteor. Soc. Japan*, **44**, 25–43.
- McBride, J. L., B. W. Gunn, G. J. Holland, T. D. Keenan, and N. E. Davidson, 1989: Time series of total heating and moistening over the Gulf of Carpentaria radiosonde array during AMEX. *Mon. Wea. Rev.*, **117**, 2701–2713.
- , N. E. Davidson, K. Puri, and G. C. Tyrrell, 1995: The flow

- during TOGA COARE as diagnosed by the BMRC tropical analysis and prediction scheme. *Mon. Wea. Rev.*, **123**, 717–736.
- Molinari, J., and S. Skubis, 1988: Calculation of consistent flux and advective terms from adjusted vertical profiles of divergence. *Mon. Wea. Rev.*, **116**, 1829–1837.
- Nishi, N., and A. Sumi, 1995: Eastward-moving disturbances near the tropopause along the equator during the TOGA COARE IOP. *J. Meteor. Soc. Japan*, **73**, 321–337.
- North, G. R., T. L. Bell, R. F. Cahalan, and F. J. Moeng, 1982: Sampling errors in the estimation of empirical orthogonal functions. *Mon. Wea. Rev.*, **110**, 75–82.
- Numagati, A., 1995: Characteristics of 4-to-20-day-period disturbances observed in the equatorial Pacific during the TOGA COARE IOP. *J. Meteor. Soc. Japan*, **73**, 353–377.
- Song, J. L., and W. M. Frank, 1983: Relationships between deep convection and large-scale processes during GATE. *Mon. Wea. Rev.*, **111**, 2145–2160.
- Takayabu, Y. N., 1994: Large-scale cloud disturbances associated with equatorial waves. Part I: Spectral features of the cloud disturbance. *J. Meteor. Soc. Japan*, **72**, 433–465.
- Thompson, R. M., S. W. Payne, E. E. Recker, and R. J. Reed, 1979: Structure and properties of synoptic-scale wave disturbances in the intertropical convergence zone of the eastern Atlantic. *J. Atmos. Sci.*, **36**, 53–72.
- Wallace, J. M., 1971: Spectral studies of tropospheric wave disturbances in the tropical western Pacific. *Rev. Geophys. Space Phys.*, **9**, 557–612.
- Wang, R., K. Fraedrich, and S. Pawson, 1995: Phase space characteristics of the tropical stratospheric quasi-biennial oscillation. *J. Atmos. Sci.*, **52**, 4482–4500.
- Yanai, M., S. Esbensen, and J. H. Chu, 1973: Determination of bulk properties of tropical cloud clusters from large-scale heat and moisture budgets. *J. Atmos. Sci.*, **30**, 611–627.